INTERFACE

rsif.royalsocietypublishing.org

Report

Cite this article: Barnoud J, Urbini L, Monticelli L. 2015 C_{60} fullerene promotes lung monolayer collapse. *J. R. Soc. Interface* **12**: 20140931.
http://dx.doi.org/10.1098/rsif.2014.0931

Received: 19 August 2014
Accepted: 15 December 2014

Subject Areas:
biophysics, nanotechnology

Keywords:
lipid monolayer, lung surfactant, nanoparticle, fullerene, molecular dynamics, coarse-grain

Author for correspondence:
Luca Monticelli
e-mail: luca.monticelli@inserm.fr

†These authors contributed equally to this work.
‡Present address: Laboratoire Biométrie et Biologie Evolutive, Université Claude Bernard Lyon I, CNRS, Villeurbanne, UMR5558, France.

Electronic supplementary material is available at http://dx.doi.org/10.1098/rsif.2014.0931 or via http://rsif.royalsocietypublishing.org.

THE ROYAL SOCIETY PUBLISHING

C_{60} fullerene promotes lung monolayer collapse

Jonathan Barnoud[1,2,†], Laura Urbini[1,2,†,‡] and Luca Monticelli[3,4]

[1]INSERM, UMR-S665, Paris 75015, France
[2]Université Paris Diderot, Sorbonne Paris Cité, UMR-S665, Paris 75013, France
[3]BMSSI, CNRS UMR 5086, IBCP, Lyon, France
[4]Université Claude Bernard Lyon I, Lyon, France

Airborne nanometre-sized pollutants are responsible for various respiratory diseases. Such pollutants can reach the gas-exchange surface in the alveoli, which is lined with a monolayer of lung surfactant. The relationship between physiological effects of pollutants and molecular-level interactions is largely unknown. Here, we determine the effects of carbon nanoparticles on the properties of a model of lung monolayer using molecular simulations. We simulate phase-separated lipid monolayers in the presence of a model pollutant nanoparticle, C_{60} fullerene. In the absence of nanoparticles, the monolayers collapse only at very low surface tensions (around 0 mN m^{-1}). In the presence of nanoparticles, instead, monolayer collapse is observed at significantly higher surface tensions (up to *ca* 10 mN m^{-1}). Collapse at higher tensions is related to lower mechanical rigidity of the monolayer. It is possible that similar mechanisms operate on lung surfactant *in vivo*, which suggests that health effects of airborne carbon nanoparticles may be mediated by alterations of the mechanical properties of lung surfactant.

1. Introduction

Air pollution is a growing concern for public health. Airborne pollutants have been shown to be responsible for cardiovascular and respiratory diseases [1–3]. So-called ultrafine particles—with a diameter smaller than 100 nm—cause most of the diseases associated with air pollution; most of these particles originate from incomplete combustion of fossil fuels and therefore they consist largely of carbon. Contrary to bigger particles, which get stuck in the upper respiratory ways, nanometre-sized particles can reach the gas-exchange surface in the alveoli [1], which is lined with a monolayer of lung surfactant [4]. Lung surfactant monolayers consist of different types of phospholipids, cholesterol and surfactant proteins [5]. Their main physiological function is to reduce the surface tension at the air–liquid interface, preventing alveolar collapse and reducing the work needed for breathing. The effect of nanoparticles *in vivo* depends on nanoparticle chemical and physical properties and on nanoparticle interaction with lung membranes, but the relationship between physiological effects and molecular-level interactions is largely unknown.

Analogous to cell membranes [6], lung monolayer membranes are laterally heterogeneous, with more rigid domains (consisting mostly of saturated lipids and cholesterol) and more fluid domains (consisting mostly of unsaturated lipids) [7,8]. During exhalation, the size of the alveoli is reduced, and their diameter can drop from 250 to 160 µm [9]. At high compression, the interfacial monolayers bend and form bilayers in the water phase—a phenomenon named monolayer collapse that has been observed both experimentally [8,10–12] and in simulations of model systems [13]. It is possible that physiological effects of nanoparticles stem from alterations of lung monolayer properties, for example the lateral organization or the mechanism of monolayer collapse. To test this hypothesis, we performed molecular dynamics simulations of phase-separated monolayers with and without a model pollutant nanoparticle. We chose C_{60} fullerene as a simple model for hydrophobic nano-sized air pollutant. Simulations of lipid monolayers in the presence of fullerene have been reported

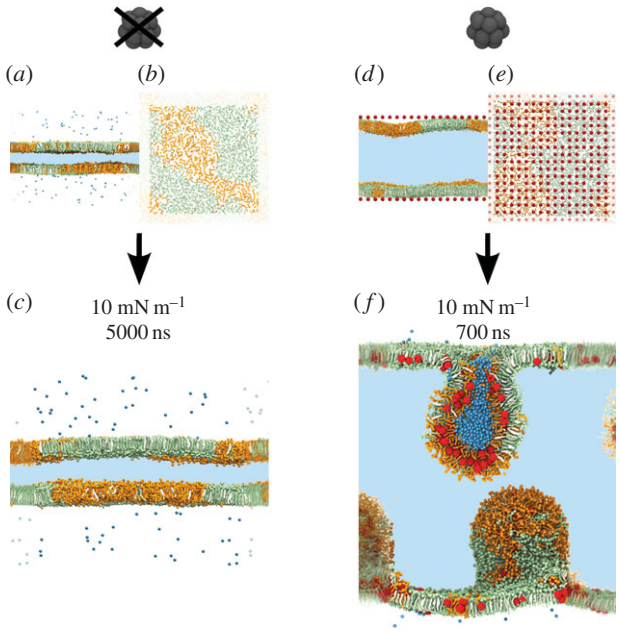

Figure 1. Starting configurations of selected systems with a surface tension (γ) of 10 mN m^{-1}: (*a*,*b*) system without fullerene, side view (*a*) and top view (*b*); (*d*,*e*) system with 10% fullerene, side view (*d*) and top view (*e*). At $\gamma = 10$ mN m^{-1}, the monolayers do not collapse in the absence of fullerene (*c*), while they do collapse rapidly in the presence of 10% fullerene (*f*). DPPC is coloured in green, DOPC in orange, cholesterol in white and fullerene in red. In the side views, the area in light blue represents the water phase. In the top views (*b*,*e*), only the lipid polar heads are represented, for the sake of clarity. Water in the vapour phase and inside the semi-vesicles is represented explicitly in blue. Periodic images are blurred. (Online version in colour.)

before [14], but only homogeneous (single lipid) monolayers were examined, and the effect of nanoparticles on monolayer collapse has never been explored in simulations before. We performed simulations at different levels of compression of a laterally heterogeneous monolayer. From the simulations, we determined both the collapse pressure and the mechanism of collapse, in the presence and in the absence of pollutant.

2. Material and methods

Our simulation system consisted of two lipid monolayers bounding a water slab (figure 1*a*). The monolayers contained a saturated lipid (dipalmitoylphosphatidylcholine, DPPC), an unsaturated lipid (dioleoylphosphatidylcholine, DOPC) and cholesterol. We used two different lipid compositions, with DPPC : DOPC : cholesterol molar ratio of 5 : 3 : 4 (2304 lipids per monolayer) or 5 : 3 : 2 (1920 lipids per monolayer). The number of water particles was 45 735 for all simulations with no monolayer collapse, and up to 184 000 in simulations with monolayer collapse (see Results). Fullerene molecules were placed in the vapour phase, in contact with the lipid tails, symmetrically distributed between the two monolayers (figure 1*d*), at two different concentrations: 3 and 10% (fullerene/lipid molar fraction). A complete list of the simulations performed is reported in table 1.

We used the MARTINI coarse-grained force field [15–17] for all simulations, with standard parameters for non-bonded interactions (cut-off of 1.2 nm, Lennard-Jones interactions shifted from 0.9 nm, Coulomb interactions shifted starting from 0 nm). The model for DOPC was modified as reported by Baoukina *et al.* [18]. It has been shown before that the MARTINI model cannot reproduce accurately the properties of lipid monolayers at low compression (i.e. high surface tension) while it can be used to explore the behaviour of monolayers at high compression (i.e. low surface tension) [19,20]. In fact, the MARTINI model has successfully been used to characterize lipid monolayer collapse upon compression [13], as well as phase coexistence in monolayer at surface tensions up to 30 mN m^{-1} [18]. For fullerene, we used the MARTINI model developed by Monticelli [21,22], which has been previously used to study fullerene aggregation in lipid bilayers and alkanes [23], and the effect of fullerene on phase separation in heterogeneous membranes [24].

We carried out the simulations at a constant temperature of 290 K, using the Bussi–Donadio–Parrinello thermostat [25] ($\tau_T = 1$ ps) and constant surface tension, using the Berendsen algorithm [26] ($\tau_P = 5$ ps, compressibility $= 5 \times 10^{-5}$ bar^{-1}). The size of the box in the direction of the monolayer normal was fixed. The analysis of lipid order parameters was carried out with in-house software (available free of charge at http://perso.ibcp.fr/luca.monticelli/; see [27]). Uncertainties were calculated using a block averaging procedure [28].

3. Results

First, we performed simulations in the absence of fullerene at surface tensions of 5, 10, 20 and 30 mN m^{-1} with both lipid compositions (5 µs sampling for each run). In all cases, the monolayers were initially phase separated (figure 1*a*,*b*), with a more ordered phase rich in saturated lipids (DPPC) and cholesterol and a more disordered phase rich in unsaturated lipids (DOPC); considering the similarity with liquid-ordered (L_o) and liquid-disordered (L_d) phases in lipid bilayers, we will use the same names in the case of monolayers. Phase separation persisted throughout the simulations at all four values of the surface tension, and no collapse was observed (figure 1*c*).

Then we compressed the monolayers to zero surface tension and observed monolayer collapse within a few tens of nanoseconds. The mechanism of collapse was similar to the one described by Baoukina *et al.* [13] on laterally homogeneous systems: the monolayer first buckled; then, it collapsed forming a bilayer in the aqueous phase; finally, the bilayer formed a semi-vesicle attached to the monolayer. Again, all systems remained phase-separated throughout the simulations. In all systems, the collapse started in the L_d phase. About 30 ns after the beginning of the collapse, all the L_d phase formed a bilayer in the water phase, and the monolayer at the liquid–vapour interface consisted almost exclusively of the L_o phase. The reproducibility of the mechanism of collapse was verified by repeating the simulations three times with different initial velocities. Our findings match very well the description of the mechanism of collapse of heterogeneous lipid monolayers recently reported by Baoukina *et al.* [29], with the collapse always starting in the L_d phase.

A mechanism of collapse with unsaturated lipids being squeezed out of the interface has been hypothesized for over three decades [30]. A number of experiments clearly support (at least partial) exclusion of unsaturated lipids from the interfacial monolayer upon collapse, and subsequent enrichment in unsaturated lipids in the collapsed bilayers [31–33]. Yet, other experimental results contradict this hypothesis [34–36]. Our simulations are consistent with preferential transfer of the L_d phase to the collapsed bilayers.

Then we repeated the simulations in the presence of fullerene, using a concentration of 3 or 10% (molar fraction with respect to the lipids), and the same surface tensions as in the absence of fullerene (5, 10, 20 and 30 mN m^{-1}). Fullerene molecules were initially placed in the vapour phase in close

Table 1. List of simulations performed.

surface tension (mN m^{-1})	fullerene concentration (% molar)	number of fullerene molecules per monolayer	duration (μs)	collapse?
high cholesterol concentration: 960 DPPC, 576 DOPC, 768 cholesterol per monolayer				
0	0	0	0.20 + 0.20 + 0.12	yes
5	0	0	5	no
10	0	0	5	no
20	0	0	5	no
30	0	0	5	no
5	3	69	0.38	yes
10	3	69	5	no
20	3	69	5	no
30	3	69	5	no
5	10	230	0.12	yes
10	10	230	0.77 + 0.22 + 0.24	yes
20	10	230	5	no
30	10	230	5	no
low cholesterol concentration: 960 DPPC, 576 DOPC, 384 cholesterol per monolayer				
0	0	0	0.12 + 1.2	yes
5	0	0	5	no
10	0	0	5	no
20	0	0	5	no
30	0	0	5	no
5	3	57	2.9	yes
10	3	57	5	no
20	3	57	5	no
30	3	57	5	no
5	10	192	0.10	yes
10	10	192	0.95	yes
20	10	192	5	no
30	10	192	5	no

proximity to the lipid acyl chains and were equally spaced, and therefore equally distributed between the L_o and L_d phase. All fullerenes permeated the monolayers very rapidly (nanosecond time scale) and remained in contact with the lipids throughout the simulations, avoiding both the water and the vapour phase. While in the lipid phase, fullerene aggregation was rather limited, and only small clusters were formed—as also observed previously in lipid bilayer systems [21,23]. Fullerene molecules redistributed preferentially to the L_d phase on a time scale of a few microseconds. To quantify fullerene lateral distribution in our monolayer systems, we calculated the fullerene–DOPC contact fraction (i.e. the fraction of contacts made by fullerene with DOPC over the contacts made by fullerene with all phospholipids). At the beginning of the simulations, the fullerene–DOPC contact fraction was close to 0.37, which is the value expected for ideal mixing (0.37 being equal to the molar fraction of DOPC). Within about 4 μs, the fullerene–DOPC contact fraction converged to values higher than 0.7, independently of surface tension, fullerene concentration and cholesterol concentration (electronic supplementary material, figure S1). Strong preferential partitioning of fullerene (and other aromatic compounds) to L_d phases has previously been observed in lipid bilayers [24].

Unlike fullerene, cholesterol distributed mainly in the L_o phase. Remarkably, cholesterol distribution was significantly affected by fullerene: for each given surface tension, the cholesterol–DOPC contact fraction decreased with increasing fullerene concentrations. In other words, fullerene appeared to exclude cholesterol from the L_d phase, in line with previous findings in lipid bilayers [24].

The most striking effect of fullerene was related to monolayer collapse. In the absence of fullerene, monolayer collapse was observed only at a surface tension of 0 mN m^{-1}, corresponding to very high lateral pressure. With 3% fullerene concentration, the monolayer collapsed already at a surface tension of 5 mN m^{-1} (and obviously also at lower surface tensions, i.e. higher lateral pressures). With 10% fullerene concentration, the monolayer collapsed at even higher surface tension, 10 mN m^{-1} (figure 1*f*). Again, simulations were repeated three times to guarantee the reproducibility of the results. We conclude that fullerene destabilizes lipid monolayers and promotes their collapse in the water phase.

To understand the molecular-level causes of monolayer destabilization by fullerene, we analysed the effect of fullerene on membrane properties. First, we examined the monolayer lateral organization, and did not observe any major change within the simulation time (5 µs). Yet, analysis of lipid–lipid contacts showed that convergence requires simulations on longer time scales; therefore, an effect of the nanoparticles on lipid domains cannot be excluded.

We then examined nanoparticle distribution, lipid ordering and orientation, and the monolayer compressibility modulus. Fullerene partitioned preferentially to the L_d phase, both before and after monolayer collapse. Therefore, one would expect an effect of fullerene on the properties of the L_d phase, for instance on lipid ordering. Contrary to intuition, fullerene had very little influence on the order of unsaturated lipid at high surface tension (30 mN m^{-1}), and no effect at all at surface tension of 20 mN m^{-1} or less (figure 2; electronic supplementary material, figure S2). Instead, fullerene did affect ordering of saturated lipid chains. At a surface tension of 20 mN m^{-1}, the average order parameter of bonds in the DPPC acyl chains decreased from 0.78 (in the absence of fullerene) to 0.74 (10% fullerene). The end of the tails, at the lipid–vapour interface, was especially affected (figure 2). In the presence of fullerene, saturated lipids tended to tilt more with respect to the membrane normal (electronic supplementary material, figure S3). Nevertheless, we did not find a direct correlation between local lipid tilt and proximity to a fullerene molecule.

Finally, we calculated the area compressibility modulus, K_A, of the monolayers from the fluctuations of monolayer area, as: $K_A = k_B T A/\sigma_A^2$, where k_B is the Boltzmann constant, T is the temperature in kelvin, A is the average area per lipid and σ_A^2 is its variance. For both monolayer compositions, we found that the compressibility modulus decreased with increasing fullerene concentration (figure 2), indicating that the nanoparticles decreased the mechanical rigidity of the monolayers—analogous to previous observations in lipid bilayers [21].

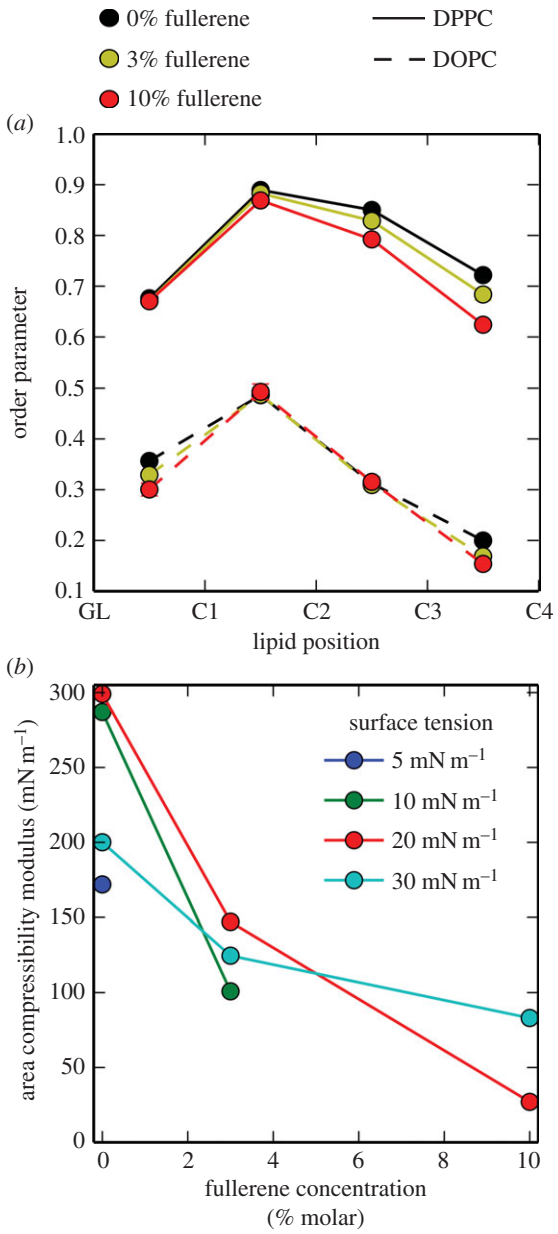

Figure 2. (*a*) Bond order parameter for each bond in the lipid chains of DPPC and DOPC at different fullerene concentration and surface tension of 20 mN m^{-1}, in the simulation with high concentration of cholesterol. (*b*) Area compressibility modulus as a function of fullerene concentration, in simulations with high concentration of cholesterol. Lines serve only as a guide to the eye. (Online version in colour.)

4. Outlook

Lipophilic nano-sized particles can partition into lipid monolayer membranes and alter their physical properties. Here, we show that pure carbon nanoparticles promote monolayer collapse by perturbing the ordering of lipid tails and decreasing the rigidity of the monolayer. As discussed in [29], the stability of lipid monolayers is enhanced in simulations (compared to experiments), so we do not expect that the surface tensions required for monolayer collapse in the simulations (i.e. the minimum surface tensions) match experimental values; yet, we expect that simulations reproduce correctly the trend of minimum surface tension versus monolayer composition [29], including the effect of nanoparticles embedded in or adsorbed onto monolayers.

Simulations reported here do not allow us to tell whether the size, the shape or the hydrophobicity of the nanoparticle is a requirement to reduce monolayer stability. Also, it is difficult to compare the quantity of nanoparticles used in our simulations with real-world nanoparticle exposure data: for airborne pollutants, exposure is usually reported as mass of pollutant per volume of air for a given exposure time, which is difficult to correlate with the actual quantity of pollutant deposited on lung membranes. In some experiments, nanoparticle suspensions were instilled intratracheally into mice [37,38] or rats [39]. In those cases, assuming that all nanoparticles deposit on lung membranes and knowing approximately the surface area of mice lungs [40], one can estimate the exposure in terms of mass of the nanoparticles per unit of lung membrane surface, or in terms of total nanoparticle surface over lung membrane surface. Considering the first metric, the exposure used in our simulations is about one order of magnitude less than in the experiments above (150–500 µg m^{-2} in our simulations, versus 1200–6000 µg m^{-2} in [37,38]), while the second metric suggests approximately equivalent exposure (the surface area of monomeric C_{60} fullerene is approximately one order of magnitude larger than the surface area of soot and ultrafine particles [37]). The nanoparticle concentrations in our simulations are therefore comparable to the ones used *in vivo* on mice.

Our model monolayers feature a composition simpler than lung surfactant membranes, yet they do contain the main components of lung surfactant (saturated phospholipids, unsaturated phospholipids and cholesterol) and show a complex lateral organization, similar to the one observed in lung surfactant extracts. Therefore, it is likely that carbon nanoparticles will affect the properties of lung surfactant membranes in a similar way, reducing monolayer rigidity and decreasing monolayer collapse pressure (i.e. increasing the minimum surface tension attainable by the monolayer), both *in vitro* and *in vivo*. While the precise mechanism of action of airborne carbon-based pollutants *in vivo* remains unclear, our simulations suggest that the effects of such particles on health may be mediated by alterations in the mechanical properties of lung surfactant.

Data accessibility. Supporting information available: additional figures, available free of charge via the Internet. Starting structure files, topologies and simulation parameters are available via Figshare (http://dx.doi.org/10.6084/m9.figshare.1241506).

Acknowledgement. The authors thank Peter Tieleman for providing the starting structures for one of the two sets of lipid monolayers and for many fruitful discussions. L.M. designed the simulations. J.B. and L.U. carried out the simulations and analyses. The manuscript was written by L.M. and J.B.

Funding statement. This work was performed using HPC resources from GENCI-CINES (grant nos. 2012-076353 and 2013-076353). L.M. acknowledges funding by the Institut National de la Santé et de la Recherche Médicale (INSERM) and the Agence nationale de sécurité sanitaire de l'alimentation, de l'environnement et du travail (ANSES, grant EST2011/096). J.B. is funded by Université Paris Diderot.

References

1. Buzea C, Pacheco I, Robbie K. 2007 Nanomaterials and nanoparticles: sources and toxicity. *Biointerphases* **2**, MR17–MR71. (doi:10.1116/1.2815690)
2. Lam CW, James JT, McCluskey R, Arepalli S, Hunter RL. 2006 A review of carbon nanotube toxicity and assessment of potential occupational and environmental health risks. *Crit. Rev. Toxicol.* **36**, 189–217. (doi:10.1080/10408440600570233)
3. Seaton A, Macnee W, Donaldson K, Godden D. 1995 Particulate air pollution and acute health effects. *Lancet* **345**, 176–178. (doi:10.1016/s0140-6736(95)90173-6)
4. Wustneck R, Perez-Gil J, Wustneck N, Cruz A, Fainerman VB, Pison U. 2005 Interfacial properties of pulmonary surfactant layers. *Adv. Colloid Interface Sci.* **117**, 33–58. (doi:10.1016/j.cis.2005.05.001)
5. Goerke J. 1998 Pulmonary surfactant: functions and molecular composition. *Biochim. Biophys. Acta* **1408**, 79–89. (doi:10.1016/S0925-4439(98)00060-X)
6. Simons K, Ikonen E. 1997 Functional rafts in cell membranes. *Nature* **387**, 569–572. (doi:10.1038/42408)
7. Discher BM, Maloney KM, Schief WR, Grainger DW, Vogel V, Hall SB. 1996 Lateral phase separation in interfacial films of pulmonary surfactant. *Biophys. J.* **71**, 2583–2590. (doi:10.1016/S0006-3495(96)79450-X)
8. Bernardino de la Serna J, Perez-Gil J, Simonsen AC, Bagatolli LA. 2004 Cholesterol rules: direct observation of the coexistence of two fluid phases in native pulmonary surfactant membranes at physiological temperatures. *J. Biol. Chem.* **279**, 40 715–40 722. (doi:10.1074/jbc.M404648200)
9. Mouritsen OG. 2004 *Life—as a matter of fat*. New York, NY: Springer.
10. Schurch S, Qanbar R, Bachofen H, Possmayer F. 1995 The surface-associated surfactant reservoir in the alveolar lining. *Biol. Neonate* **67**, 61–76. (doi:10.1159/000244207)
11. Piknova B, Schram V, Hall SB. 2002 Pulmonary surfactant: phase behavior and function. *Curr. Opin. Struct. Biol.* **12**, 487–494. (doi:10.1016/s0959-440x(02)00352-4)
12. Amrein M, von Nahmen A, Sieber M. 1997 A scanning force and fluorescence light microscopy study of the structure and function of a model pulmonary surfactant. *Eur. Biophys. J. Biophys. Lett.* **26**, 349–357. (doi:10.1007/s002490050089)
13. Baoukina S, Monticelli L, Risselada HJ, Marrink SJ, Tieleman DP. 2008 The molecular mechanism of lipid monolayer collapse. *Proc. Natl Acad. Sci. USA* **105**, 10 803–10 808. (doi:10.1073/pnas.0711563105)
14. Chiu C-C, Shinoda W, DeVane RH, Nielsen SO. 2012 Effects of spherical fullerene nanoparticles on a dipalmitoyl phosphatidylcholine lipid monolayer: a coarse grain molecular dynamics approach. *Soft Matter* **8**, 9610–9616. (doi:10.1039/c2sm26357b)
15. Marrink SJ, de Vries AH, Mark AE. 2004 Coarse grained model for semiquantitative lipid simulations. *J. Phys. Chem. B* **108**, 750–760. (doi:10.1021/jp036508g)
16. Marrink SJ, Risselada HJ, Yefimov S, Tieleman DP, de Vries AH. 2007 The MARTINI force field: coarse grained model for biomolecular simulations. *J. Phys. Chem. B* **111**, 7812–7824. (doi:10.1021/jp071097f)
17. Monticelli L, Kandasamy SK, Periole X, Larson RG, Tieleman DP, Marrink SJ. 2008 The MARTINI coarse-grained force field: extension to proteins. *J. Chem. Theory Comput.* **4**, 819–834. (doi:10.1021/ct700324x)
18. Baoukina S, Mendez-Villuendas E, Tieleman DP. 2012 Molecular view of phase coexistence in lipid monolayers. *J. Am. Chem. Soc.* **134**, 17 543–17 553. (doi:10.1021/ja304792p)
19. Baoukina S, Monticelli L, Marrink SJ, Tieleman DP. 2007 Pressure–area isotherm of a lipid monolayer from molecular dynamics simulations. *Langmuir* **23**, 12 617–12 623. (doi:10.1021/la702286h)
20. Duncan S, Larson R. 2008 Comparing experimental and simulated pressure-area isotherms for DPPC. *Biophys. J.* **94**, 2965–2986. (doi:10.1529/biophysj.107.114215)
21. Wong-Ekkabut J, Baoukina S, Triampo W, Tang IM, Tieleman DP, Monticelli L. 2008 Computer simulation study of fullerene translocation through lipid membranes. *Nat. Nanotechnol.* **3**, 363–368. (doi:10.1038/nnano.2008.130)
22. Monticelli L. 2012 On atomistic and coarse-grained models for C_{60} fullerene. *J. Chem. Theory Comput.* **8**, 1370–1378. (doi:10.1021/ct3000102)
23. Barnoud J, Rossi G, Monticelli L. 2014 Lipid membranes as solvents for carbon nanoparticles. *Phys. Rev. Lett.* **112**, 068102. (doi:10.1103/PhysRevLett.112.068102)
24. Barnoud J, Rossi G, Marrink SJ, Monticelli L. 2014 Hydrophobic compounds reshape membrane domains. *PLoS Comput. Biol.* **10**, e1003873. (doi:10.1371/journal.pcbi.1003873)
25. Bussi G, Donadio D, Parrinello M. 2007 Canonical sampling through velocity rescaling. *J. Chem. Phys.* **126**, 014101. (doi:10.1063/1.2408420)
26. Berendsen HJC, Postma JPM, van Gunsteren WF, di Nola A, Haak JR. 1984 Molecular dynamics with coupling to an external bath. *J. Chem. Phys.* **81**, 3684–3690. (doi:10.1063/1.448118)
27. Castillo N, Monticelli L, Barnoud J, Tieleman DP. 2013 Free energy of WALP23 dimer association in DMPC, DPPC, and DOPC bilayers. *Chem. Phys. Lipids* **169**, 95–105. (doi:10.1016/j.chemphyslip.2013.02.001)
28. Hess B. 2002 Determining the shear viscosity of model liquids from molecular dynamics simulations. *J. Chem. Phys.* **116**, 209–217. (doi:10.1063/1.1421362)
29. Baoukina S, Roznnanov D, Mendez-Villuendas E, Tieleman DP. 2014 The mechanism of collapse of heterogeneous lipid monolayers. *Biophys. J.* **107**, 1136–1145. (doi:10.1016/j.bpj.2014.05.053)
30. Bangham AD, Morley CJ, Phillips MC. 1979 Physical properties of an effective lung surfactant. *Biochim. Biophys. Acta* **573**, 552–556. (doi:10.1016/0005-2760(79)90229-7)
31. Pastrana-Rios B, Flach CR, Brauner JW, Mautone AJ, Mendelsohn R. 1994 A direct test of the squeeze-out hypothesis of lung surfactant function—external reflection FT-IR at the air/water interface. *Biochemistry* **33**, 5121–5127. (doi:10.1021/bi00183a016)
32. Takamoto DY, Lipp MM, von Nahmen A, Lee KYC, Waring AJ, Zasadzinski JA. 2001 Interaction of lung surfactant proteins with anionic phospholipids.

Biophys. J. **81**, 153–169. (doi:10.1016/S0006-3495(01)75688-3)

33. Keating E, Zuo YY, Tadayyon SM, Petersen NO, Possmayer F, Veldhuizen RA. 2012 A modified squeeze-out mechanism for generating high surface pressures with pulmonary surfactant. *Biochim. Biophys. Acta* **1818**, 1225–1234. (doi:10.1016/j.bbamem.2011.12.007)
34. Lipp MM, Lee KYC, Takamoto DY, Zasadzinski JA, Waring AJ. 1998 Coexistence of buckled and flat monolayers. *Phys. Rev. Lett.* **81**, 1650–1653. (doi:10.1103/PhysRevLett.81.1650)
35. Piknova B, Schief WR, Vogel V, Discher BM, Hall SB. 2001 Discrepancy between phase behavior of lung surfactant phospholipids and the classical model of surfactant function. *Biophys. J.* **81**, 2172–2180. (doi:10.1016/S0006-3495(01)75865-1)
36. Bourdos N, Kollmer F, Benninghoven A, Ross M, Sieber M, Galla HJ. 2000 Analysis of lung surfactant model systems with time-of-flight secondary ion mass spectrometry. *Biophys. J.* **79**, 357–369. (doi:10.1016/S0006-3495(00)76297-7)
37. Stoeger T, Reinhard C, Takenaka S, Schroeppel A, Karg E, Ritter B, Heyder J, Schulz H. 2006 Instillation of six different ultrafine carbon particles indicates a surface area threshold dose for acute lung inflammation in mice. *Environ. Health Perspect.* **114**, 328–333. (doi:10.1289/ehp.8266)
38. Shvedova AA *et al*. 2005 Unusual inflammatory and fibrogenic pulmonary responses to single-walled carbon nanotubes in mice. *Am. J. Physiol. Lung Cell. Mol. Physiol.* **289**, L698–L708. (doi:10.1152/ajplung.00084.2005)
39. Shinohara N *et al*. 2010 Clearance kinetics of fullerene C_{60} nanoparticles from rat lungs after intratracheal C_{60} instillation and inhalation C_{60} exposure. *Toxicol. Sci.* **118**, 564–573. (doi:10.1093/toxsci/kfq288)
40. Knust J, Ochs M, Gundersen HJG, Nyengaard JR. 2009 Stereological estimates of alveolar number and size and capillary length and surface area in mice lungs. *Anat. Rec. Adv. Integr. Anat. Evol. Biol.* **292**, 113–122. (doi:10.1002/ar.20747)